ASDJ
AINSHAMS DENTAL JOURNAL

Print ISSN 1110-7642
Online ISSN 2735-5039

AIN SHAMS DENTAL JOURNAL
Official Publication of Ain Shams Dental School
June2025 • Vol. 38

Effect of Green synthesized Silver Nanoparticles Using Pisum Sativum Peel Aqueous Extract on Oral Squamous Cell Carcinoma, Oral Epithelial cells and Fibroblasts cell lines

Basma Abdelrahman Ahmed [1], Rania Osama M. Mohsen[2], Mai Hafez Mohamed[2]

Aim: Evaluate the cytotoxic effect of green synthesized silver nanoparticles (AgNPs) using Pisum sativum (PS) outer peel on oral squamous cell carcinoma cell line (HNO97), and their safety on normal oral epithelial cells (OEC) and human skin fibroblasts (HSF).
Materials and Methods: Green synthesis of AgNPs from PS and their characterization were performed. IC50 doses after 24h and 48h on HNO97, OEC and HSF cell lines were calculated. The study groups were divided into control untreated groups: HNO97-C, OEC-C, HSF-C, and treated (T) groups: HNO97-T OEC-T, HSF-T that were treated with AgNPs IC50 dose of HNO97 after 48h. The effect of Pisum sativum silver nanoparticles (PS-AgNPs) on cell lines morphology, nuclear area factor (NAF), proliferating cell nuclear antigen (PCNA), transforming growth factor beta 1 (TGFβ1), caspase 3, and reactive oxygen species (ROS) production was detected.
Results: The IC50 values of PS-AgNPs for HNO97 were 87.60 µg/ml and 35.07 µg/ml after 24h and 48h respectively, and being significantly higher in OEC and HSF. Treating all cell lines with PS-AgNPs IC50 dose of HNO97 after 48h revealed significant morphological apoptotic changes in HNO97 with no obvious changes in OEC and HSF. There was a statistically significant reduction in NAF, besides PCNA and TGFβ1 fold change, and statistically significant rise in caspase 3 and ROS production in HNO97-T compared to HNO97-C group, while there were no statistically significant differences in OEC-T and HSF-T when compared to their control groups.
Conclusion: PS-AgNPs are cytotoxic to OSCC while being safe on normal OEC and HSF.

Keywords: Pisum sativum synthesized silver nanoparticles; PCNA; TGFβ1; Caspase 3, Nuclear area factor.

1. Oral Pathology Department, Faculty of Dentistry, Ain Shams University, Cairo, Egypt.
2. Oral Biology Department, Faculty of Dentistry, Ain Shams University, Cairo, Egypt
3. Oral Pathology Department, Faculty of Dentistry, British University in Egypt
Corresponding author: Rania Osama M. Mohsen, email: dr.rania.osama@dent.asu.edu.eg

Introduction

Oral Squamous Cell Carcinoma (OSCC) is the most prevalent oral cavity malignant tumor all over the world.[1] OSCC pathogenicity is related to several factors as genetic, epigenetic, and environmental factors that can result in gene mutations in normal epithelial cells.[2]

Oral epithelial cells (OEC) perform a crucial role as being the primary protective barrier of oral mucosa against microorganisms, toxic materials, or mechanical damage, in addition to thermal regulation and various inflammatory mediators' secretion.[3] Fibroblasts are considered one of the most principal cells in the connective tissue. The chief function of fibroblasts is the synthesis of collagen and extracellular matrix as well as their metabolism, in addition to their contribution to epithelial differentiation, wound healing, regulation of inflammation, and various growth factors secretion.[4,5]

Earlier, the physical and chemical approaches for nanomaterials synthesis were performed by using toxic chemicals and complicated reaction conditions, that tend to produce biohazards in the environment. The concept of nanotechnology aimed to generate nanomaterials that are potentially safe for the environment.[6] Nanoparticles synthesized via a 'green' approach using biological materials such as various plant extracts, algae, fungi, and other beneficial microorganisms as the reducing agents in the synthesis process, have been documented in many studies.[7-9] The green nanotechnology to synthesize nanoparticles such as silver, gold, palladium, and platinum, provides merits over the conventional methods by being an environment-friendly and cost-effective approach.[7,8] These prepared metal nanoparticles compete with chemical methodologies according to their size and shape as well as having advanced properties.[6]

Lately, the green synthesis of metal nanoparticles can be executed by using kitchen household waste like the peels of fruits and vegetables as the reducing agents in the synthesis process.[10, 11] The food waste materials utilization for synthesizing different nanoparticles has been a highly effective, environmental-friendly and low-cost method for waste recycling that is used in biomedicines and pharmaceuticals generation.[12] The seeds of a pea (Pisum sativum) (PS) are only edible and their peel is disposed of as a waste. The pea peel is rich in natural bioactive components with antimicrobial, antioxidant, and anticancer potential. Besides, it has been reported that peel waste can be used as a reducing agent in nanoparticle synthesis.[12-14]

Silver nanoparticles (AgNPs) have been accounted as a beneficial novel platform for different therapeutic purposes.[6] AgNPs exhibit several biological potentials as anti-inflammatory, antioxidant, antiviral, and anti-microbial activities.[9, 15] Furthermore, because of the enhanced permeability and retention of the nanoparticles, they display better accumulation at tumor sites, being a promising agent for replacing traditional chemotherapy.[16]

This study aimed to evaluate the cytotoxic effect of green synthesized AgNPs by PS outer peel on OSCC (HNO97) cell line, and their safety on normal OEC and human skin fibroblasts (HSF) cell lines. In addition, to detect the effect of Pisum sativum silver nanoparticles (PS-AgNPs) on proliferation, transforming growth factor beta 1 (TGFβ1), apoptosis, and reactive oxygen species (ROS) production.

Materials and Methods

Chemicals and Reagents

The PS-AgNPs were prepared in Nanogate Company, Cairo, Egypt. Silver nitrate (AgNO3) and Polyvinylpyrrolidone (PVP) 40 KDa were purchased from

Millipore Merck (Darmstadt, Germany). iScript™ One-Step Reverse Transcription-Quantitative Polymerase Chain Reaction (RT-qPCR) Kit with SYBR® Green was obtained from Bio-Rad, CA, USA. Proliferating cell nuclear antigen (PCNA) gene primer (HP206250): Hs_PCNA_1_SG, TGFβ1 gene primer (HP200609): Hs_TGFβ_1_SG QuantiTect, the beta-actin (ACTB) Housekeeping gene (HP 204660): Hs_ACTB_1_SG QuantiTect gene primers were purchased from ORIGENE Company, China. Caspase 3 (Catalog No. KHO1091) and ROS (Catalog No. AMS.E01R0021), Enzyme-linked immunosorbent assay (ELISA) kits were obtained from invitrogen, CA, USA. HNO97, OEC, and HSF cell lines were obtained from Nawah Scientific, Cairo, Egypt.

Green synthesis of AgNPs using PS peel Aqueous Extract

Preparation of Peel Extract of PS

The PS vegetable peels were collected and washed with tap water (2-3 times), then rinsed with deionized water for impurities and dust removal. To remove any moisture from the peels, they were shade-dried for 10 days.

The dried peels of PS were ground into powder. To get the plant extract; 30 g of the powdered peels were boiled in 300 ml deionized water at 60°C for 40 min, then left beyond. After 3h, the color of the solution changed from colorless to yellow after boiling. For aqueous extract separation, the boiled content was filtered by Buckner funnel with the help of a vacuum pump and Whatman filter paper no.1. Finally, the PS aqueous extracts were stored in Borosil glass flasks at 4°C until needed.[11]

Synthesis of PS-AgNPs

For the preparation of PS-AgNPs, 1 mM AgNO3 in an aqueous solution was formed with 2% PVP. For the reduction of silver-to-silver ions; 1.5 ml of the PS peel extract was used as a reducing agent by being added to 50 ml of the aqueous solution of AgNO3. After boiling the solution for 30 min at 65°C, it was left at room temperature for 24h incubation period. The change in the solution color from light yellow to reddish brown verified the formation of AgNPs.[11]

Characterization of PS-AgNPs

Optical Properties

Ocean Optics *USB2000+VIS-NIR* Fiber optics spectrophotometer was used to obtain the Ultraviolet-Visible (UV-Vis) absorption spectra of the synthesized PS-AgNPs.

Transmission Electron Microscope (TEM)

The size of the obtained PS-AgNPs was determined by JEOL JEM-2100 high-resolution TEM at an accelerating voltage of 200 kV.

Fourier Transform Infrared Spectroscopy (FT-IR) Analysis

The FT-IR spectra of the prepared PS-AgNPs were obtained using an FT-IR spectrophotometer (Spectrum Two™ FT-IR Spectrometer; PerkinElmer, Waltham, MA, USA) at wavelengths ranging from 400 to 4000 cm^{-1}. Then, a graph was plotted after recording the values.[17]

Cell culture and MTT Cytotoxicity Assay

The cell lines (HNO97, OEC, and HSF) were cultured in Dulbecco-modified eagle's (DMEM) medium containing antibacterial and antifungal agents. Cells were seeded in a 96-well cell culture plate (cells density 1.2 – 1.8 × 10,000 cells/well) in a volume of 100µl complete growth medium and incubated at 37°C for 24h. A blank well containing only medium without cells was included in each test. Serial concentrations; (1000, 500, 250, 125, 62.5, 31.25, 15.6, 7.8, 3.95, 1.95, 0.95, 0.45) µg/ml of the prepared PS-AgNPs were added individually. 16 wells were used for

each concentration and the plates were incubated for 24h and 48h at 37ºC.

The plates were then removed from the incubator, examined by an inverted microscope, and transferred to a sterile work area for the MTT assay that was done according to the manufacturer's protocol.[18] ROBONIK P2000 Elisa Reader measured the absorbance at a wavelength of 450 nm. The IC50 doses after 24h and 48h of each cell line were calculated and the PS-AgNPs IC50 dose of HNO97 after 48h was the dose used for further assessments.

The study comprised six groups where each cell line was divided into two groups as follows:

• Control (C) untreated groups: HNO97-C, OEC-C, and HSF-C.

• Treated (T) groups; the cell lines were treated with the PS-AgNPs IC50 dose of HNO97 after 48h: HNO97-T, OEC-T, and HSF-T.

Hematoxylin and Eosin (H&E) Staining

For the detection of the morphological changes of the cells and nuclear area factor (NAF) measurement, the cell pellet of each group was spread on a microscopic slide, fixed with methanol 10%, and then stained with H&E. Six images of different fields in each slide with magnification 1000X oil immersion were taken by the digital camera mounted on the light microscope.

Nuclear Area Factor (NAF) Measurement

The captured images were analyzed for NAF. Briefly, the surface area and circularity of the nuclei in each field were obtained using Image J, 1.41a software, and multiplied, and then the mean NAF of the cells in each field was obtained for statistical analysis.

RNA Extraction and Reverse Transcription-Quantitative Polymerase Chain Reaction (RT-qPCR) Analysis

The RT-qPCR was performed to determine the mRNA levels of PCNA, TGFβ1, and the ACTB, which was utilized as a reference to normalize the values expressions in the HNO97, OEC, and HSF cell lines.[19] The nucleic acid sequences of the forward (F) and reverse (R) primers are illustrated in (Table 1).

Table 1: Primer sequences for RT-qPCR.

Gene	Primer Sequence	
PCNA	F	5'CAAGTAATGTCGATAAAGAGGAGG3'
	R	5' GTGTCACCGTTGAAGAGAGTGG3'
TGFβ1	F	5'TACCTGAACCCGTGTTGCTCTC3'
	R	5'GTTGCTGAGGTATCGCCAGGAA3'
ACTB	F	5'CACCATTGGCAATGAGCGGTTC3'
	R	5 'AGGTCTTTGCGGATGTCCACGT3'

The IC50 dose of PS-AgNPs was applied to the cells and then incubated for 48h. The total RNA was extracted utilizing the RNeasy Protect Mini Kit. Then, the reverse transcription was generated using an iScript™ One-Step RT-qPCR Kit with SYBR® Green, according to the manufacturer's protocol. Melting curves were performed and the relative expression levels of PCNA and TGFβ1 were calculated and normalized to ACTB in each sample using a double delta crossing threshold (ΔΔCT) method.

Enzyme-Linked Immunosorbent Assay (ELISA) Analysis

The expression of caspase 3 and ROS in each cell line was evaluated with ELISA. HNO97, OEC, and HSF cell lines were

seeded into the plates at a density of at a density of 2 × 10^6. Following overnight incubation, the cells were treated with the 48h- IC50 dosage of PS-AgNPs. Then the culture supernatants were collected, and centrifuged to pellet any detached cells. The cells were then centrifuged for 5 min at 1800×*g*, and washed with phosphate-buffered saline (PBS) after removal of media, then, the cell pellets were lysed in cold lysis buffer and centrifuged at 12,000×g for 1 min at 4°C. The supernatant was obtained to detect the protein levels of the markers and the color produced in each sample was recorded at 405 nm by a microplate reader. A standard curve was plotted and the concentration of proteins corresponding to the mean absorbance was calculated.[20]

Statistical Analysis

The data were expressed as mean ± standard deviation. T-Test was the used test for comparing the results between treated and untreated cells in each cell line. Microsoft Excel 2007 was employed in the analysis. *P* values < 0.05 were considered statistically significant.

Results:

Characterization of PS-AgNPs

The UV-Vis spectral analysis of PS-AgNPs detected an absorbance of the nanoparticles at ~422 nm. TEM results revealed that the average size of the PS-AgNPs was 20 nm and the particles were spherical. The FT-IR analysis detected absorbance peaks of the PS-AgNPS at 713.99, 1645.51, 1980.93, 2112.09, 2162.14, and 3389.91 cm^{-1} positions (Fig. 1).

Cell Viability and Determination of IC50

The MTT cell viability assay results and IC50 calculation of PS-AgNPs on OSCC, OEC, and HSF cell lines were 87.60, 536.48, and 710.03µg/ml after 24h and 35.07, 521.65, and 689.60µg/ml after 48h respectively (Fig. 2)

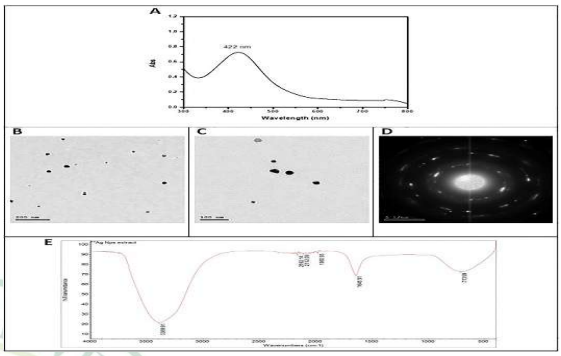

Fig. 1. Characterization of the synthesized PS-AgNPs; (A)- UV-Vis Absorption spectrum. (B, C, D)- TEM photomicrographs. (E)- FT-IR spectra from 400 cm^{-1} to 4000 cm^{-1}.

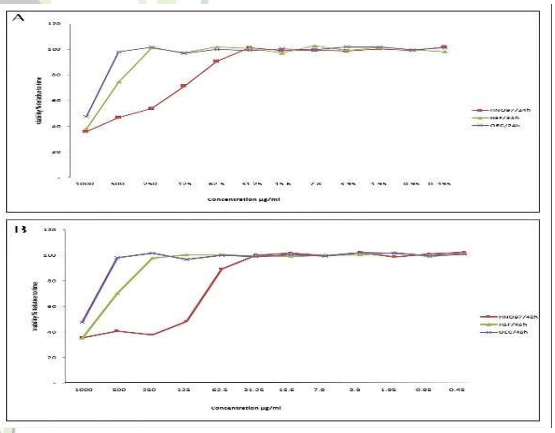

Fig. 2. Photomicrographs showing IC50 of PS-AgNPs on HNO97, OEC and HSF at (A)- 24h, and (B)- 48h.

Hematoxylin and Eosin (H&E)

Treating the HNO97 cell line with the PS-AgNPs IC50 dose of HNO97 after 48h revealed an apparent cellular morphological apoptotic change. The untreated HNO97 cell line showed sheets of confluent cells with dysplastic changes of cellular and nuclear pleomorphism and nuclear hyperchromatism (Fig. 3A). The treated HNO97 cells showed early and late apoptotic signs of cellular and nuclear shrinkage, irregular cell membrane, membrane blebbing, peripheral chromatin

condensation, chromatin fragmentation, and apoptotic bodies (Fig. 3B). In OEC-C cell line, the cells were polyhedral and preserved the adhesion between the neighboring cells (Fig. 3C). HSF-C cell line exhibited regular cells with normal morphology (Fig. 3E). No obvious morphological changes were detected in OEC and HSF cell lines after treatment (Fig. 3D, 3F).

Nuclear Area Factor (NAF)

The PS-AgNPs IC50 doses of HNO97 on HNO97, OEC, and HSF cell lines caused a highly statistically significant reduction in NAF in the HNO97-T group when compared to the untreated control ($p<0.001$). Conversely, no statistically significant difference was detected between OEC-T and HSF-T groups in comparison to their control groups (Fig. 4A).

ReverseTranscription-Quantitative Polymerase Chain Reaction (RT-qPCR)

Applying the PS-AgNPs IC50 doses of HNO97 on the different cell lines after 48h revealed a statistically significant reduction in PCNA and TGFβ1 fold change in HNO97-T group from the untreated HNO97-C group (P =0.001, <0.001 respectively), however no statistically significant reduction in PCNA and TGFβ1 fold change in OEC-T and HSF-T was observed when compared to OEC-C and HSF-C untreated groups (Fig. 4B, 4C).

Enzyme-Linked Immunosorbent Assay (ELISA)

Treatment with the PS-AgNPs IC50 doses of HNO97 on the different cell lines after 48h revealed a statistically significant rise in caspase 3 in the HNO97-T group when compared to the HNO97-C group (P=0.04). Regarding ROS, a statistically significant increase in ROS was observed in HNO97-T (P=0.02). No statistically significant difference in caspase 3 and ROS values was detected in OEC-T and HSF-T compared to their untreated control (Fig. 4D, 4E).

Discussion

Green synthesis of the AgNPs from food waste materials and plant extracts is always a good substitute for chemically reduced NPs.[21,22] PS outer peels are wastes rich in phenolic compounds and flavonoids rendering them efficient reducing agents for AgNP synthesis.[12,14] The antibacterial and cytotoxic roles of the green synthesized AgNPs from PS peel aqueous extract were proven previously[12]; however, our work was the first to detect their anticancer effect on OSCC and safety on normal OEC and HSF cell lines.

In the present study, TEM data of the nanoparticles produced from the PS outer leaf aqueous extract revealed average-sized 20 nm spherical-shaped particles. Similar to our study, Patra et al.[12] revealed a size range of the nanoparticles from 15-25nm. The UV-Vis absorption spectroscopy results demonstrated a surface plasmon resonance band due to the excitation of free electrons at 422 nm which fits the range of complete synthesis of AgNPs.[23]

The FT-IR results of AgNPs reduced by PS peel extract herein confirmed the presence of an absorbance peak at 713.99 cm^{-1} indicating stretching vibration of benzene derivative. The absorbance peak at 1645.51 cm^{-1} represented C=N stretching vibrations of imine/oxime, C=C alkene, C=C conjugated alkene, N-H bending amine, C=C cyclic alkene, and C=C alkene. The peak at 1980.93 and 2112.09 cm^{-1} referred to C=C=C allene and C≡C alkyne stretching vibrations respectively. The peak of S-C≡N thiocyanate stretching vibration appeared at 2162.14, while the peak at 3389.91 cm^{-1} belongs to O-H alcohol and N-H primary amine stretching vibration.[24]

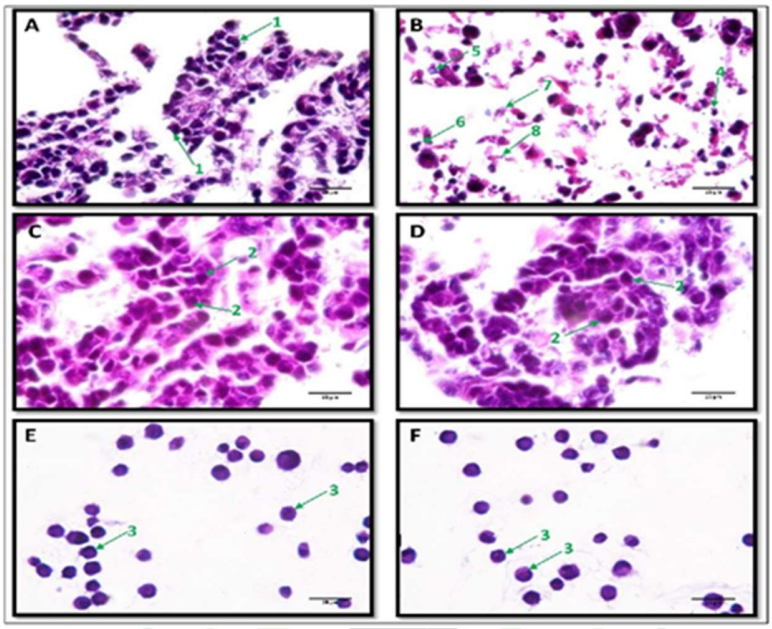

Fig. 3. Photomicrographs showing the cell lines; the control (C) and treated (T) groups with PS-AgNPs IC50 dose of HNO97 after 48h; (A)- HNO97-C, (B)- HNO97-T, (C)- OEC-C, (D)- OEC-T, (E)- HSF-C, (F)- HSF-T. (1) Confluent dysplastic pleomorphic malignant HNO97 cells, (2) Polyhedral confluent OEC cells, preserving the adhesion between the neighboring cells, (3) Regular HSF cells with normal morphology, (4) Shrunken apoptotic cell with irregular cell membrane, (5) Peripheral condensation of chromatin,(6) Membrane blebbing, (7) Nuclear fragmentation, (8) Apoptotic bodies (H&E, 1000X, Oil).

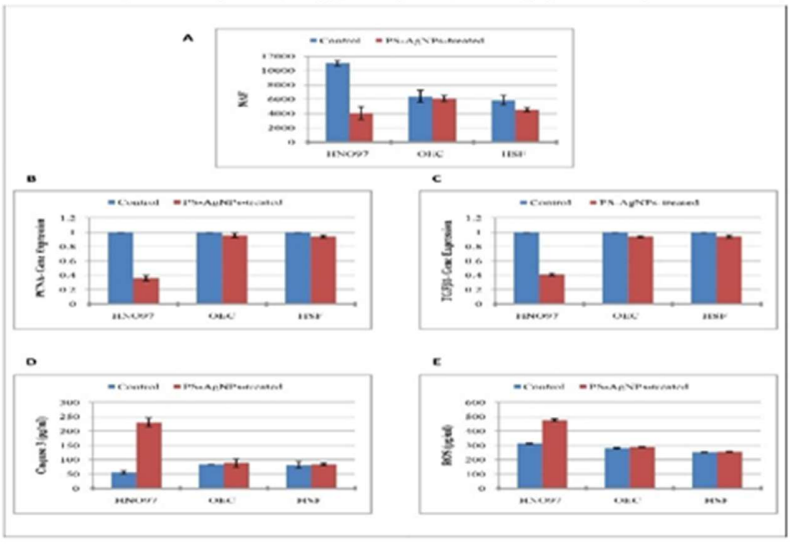

Fig. 4. Bar charts showing HNO97, OEC, and HSF control cell lines and after treatment by IC50 of PS-AgNPs regarding; (A)- NAF, (B, C)- RT-qPCR fold changes of PCNA and TGFβ1 respectively, and (D, E)- ELISA results of caspase 3 and ROS respectively

The results of this study revealed that the IC50 doses of PS-AgNPs were significantly higher in OEC and HSF when compared to that of HNO97 after 24h and 48h, explaining the selective cytotoxicity of the nanoparticles on cancer cells. The cytotoxic effect of AgNPs was attributed to their small particle size facilitating their accumulation in cell organelles.[25] The IC50 dose of PS-AgNPs after 48h on the HNO97 cell line was chosen for the other investigations to further explore the anticancer effect on OSCC and the safety on normal OEC and HSF cell lines.

Proliferating cell nuclear antigen is a protein essential for DNA replication and cell survival which was verified effective to be targeted in the highly proliferating malignancies.[26] TGFβ was proved to be linked to epithelial-mesenchymal transition of epithelial malignancy, cancer stemness, and tumor angiogenesis.[27] The results of our research revealed a statistically significant reduction in PCNA and TGFβ1 fold change in the HNO97 cell line after treatment with the IC50 dose of PS-AgNPs. The role of green synthesized AgNPs in inhibiting cancer cell proliferation was related to the ability of those nanoparticles to arrest the cell cycle in the G1 phase.[28] In an earlier study on breast and lung cancer cell lines, Mfouo-Tynga et al.[29]detected the effect of AgNPs in reducing proliferation when used in combination with laser; however, they did not find a significant anti-proliferative effect of AgNPs when used alone. The variability from our results is attributed to the difference in doses as they did not use the IC50 doses, besides the different cell lines. Acute exposure of colon, lung, mammary, and esophageal tissues to AgNPS reduced epithelial TGFβ1 secretion and cellular migration.[30]

Caspase 3 is a major executioner caspase in intrinsic and extrinsic pathways of apoptosis. Thus, increasing caspase 3 activity is generally considered an incontrovertible marker for cancer treatment efficacy.[31] Similar to our findings, green synthesized AgNPs were previously reported to induce cytotoxicity in cancer cells by promoting ROS production, activating caspase 3, forming apoptotic bodies and DNA breaks.[32] When AgNPs penetrate the cell membrane, they trigger ROS generation and reduction of glutathione level, leading to activation of crucial signal pathway proteins like nuclear factor kB (NF-kB), tumor necrosis factor-alpha (TNF-α), c-JunNH2 terminal kinase (JNK) causing cellular organelles damage, apoptotic bodies and activation of caspase 3 dependent apoptosis.[32-34] AgNPs produced by the green way of synthesis were found effective in inducing caspase 3 in lung carcinoma.[35] Banerjee et al.[36] detected apoptotic bodies, a rise in caspase 3 and 9, and induction of apoptosis in breast cancer after treatment by AgNps synthesized from the leaf extract of the mint plant.

The anticancer effect of PS-AgNPs herein was also influenced by the cytotoxic and apoptotic roles of the phenolic compounds of the PS outer peal-reducing agent. El-Feky et al.[14] reported that the phenolics of PS outer peal especially Apigenin up-regulated the pro-apoptotic genes BAX and caspase 7, while down-regulated the anti-apoptotic gene BCL-2 in breast and colon cancer.

The IC50 dose of PS-AgNPs of the HNO97 cell line did not cause any significant effect on PCNA, TGFβ1, caspase 3, and ROS in OEC and HSF cell lines. Similarly, Sayed et al.[37] documented that the application of AgNPs on normal human melanocytes had no significant influence on caspase 3 gene-level expression. Furthermore, Kumari et al.[38] revealed selective cytotoxicity of AgNPs prepared from Pinus roxburghii bioactive fraction against human prostate carcinoma and lung adenocarcinoma, while lacking toxicity toward human blood lymphocytes and breast epithelial cells. Additionally,

Artiukh et al.[39] detected cytotoxicity of natural resin-coated AgNPs on Hep2 cells with safety on normal rat kidney cells.

The safety of AgNPs on normal cell lines might be related to the difference in the concentrations of free silver ions released in normal and cancer cells which is linked to the pH of these cells. Consequently, there is a huge release of silver ions in the acidic pH of cancerous cells which affects important cellular processes, proving the selective killing of cancer cells.[40,41]

One limitation of this work is that it unveiled the effect of PS-AgNPs in only one oral cancer cell line. So, it is recommended to perform further studies on the effect of PS-AgNPs in other cell lines, besides detecting their effect on more proliferative, apoptotic, and metastatic genes, as well as other pathways of carcinogenesis. Further, loading the traditional cancer chemotherapeutic agents on PS-AgNPs could be the next step to reveal the efficiency of those nanoparticles in carrying cancer drugs and aid them in targeting the cancerous cells.

Conclusion

The PS-AgNPs can successfully target OSCC. They act by inhibiting proliferation through affecting the gene expression of PCNA as well as repressing TGFβ1 expression, besides promoting apoptosis and ROS production while being safe on normal OEC and HSF cell lines.

Ethical statement

This research was exempted by the "Research Ethics Committee" Faculty of Dentistry, Ain Shams University, Cairo, Egypt: (FDASU-Rec ER122307).

Funding

This research is Self-funded.

Declaration of Interest

There is no conflict of interest.

References

1. Chamoli A, Gosavi AS, Shirwadkar UP, Wangdale KV, Behera SK, Kurrey NK, et al. Overview of oral cavity squamous cell carcinoma: Risk factors, mechanisms, and diagnostics. Oral. Oncol. 2021; 121:105451.
2. Vineis P, Wild CP. Global cancer patterns: causes and prevention. Lancet. 2014; 383 (9916):549-57.
3. Russo FB, Pignatari GC, Fernandes IR, Dias JL, Beltrão-Braga PC. Epithelial cells from oral mucosa: How to cultivate them? Cytotechnology. 2016; 68(5):2105-14.
4. Fernandes IR, Russo FB, Pignatari GC, Evangelinellis MM, Tavolari S, Muotri AR, et al. Fibroblast sources: where can we get them? Cytotechnology. 2016; 68(2):223-8.
5. Girsang E, Lister INE, Ginting CN, Nasution SL, Suhartina S, Munshy UZ, et al. Antioxidant and anti-inflammatory activity of chlorogenic acid on lead-induced fibroblast cells. J. Phys. 2019; 1374: 1-8.
6. Sankar R, Karthik A, Prabu A, Karthik S, Shivashangari KS, Ravikumar V. Origanum vulgare mediated biosynthesis of silver nanoparticles for its antibacterial and anticancer activity. Colloids Surf B Biointerfaces. 2013; 108:80-4.
7. Veerasamy R, Xin TZ, Gunasagaran S, Xiang TFW, Yang EFC, Jeyakumar N, et al. Biosynthesis of silver nanoparticles using mangosteen leaf extract and evaluation of their antimicrobial activities. J Saudi Chem Soc. 2011; 15(2):113-20.
8. Patra JK, Baek KH. Green nanobiotechnology: factors affecting synthesis and characterization techniques. J Nanomater. 2014; 2014:219.
9. Yu Chen, Tang J, Liu X, Ren X, Zhen M, Wang L. Green biosynthesis of silver nanoparticles using Eriobotrya japonica (Thunb.) leaf extract for reductive catalysis. Materials. 2019; 12(1):189.
10. Samaddar P, Ok YS, Kim K-H, Kwon EE, Tsang DC. Synthesis of nanomaterials from various wastes and their new age applications. J Clean Prod. 2018; 197:1190-209.
11. Deepa, Ameen F, Islam MA, Dhanker R. Green synthesis of silver nanoparticles from vegetable waste of pea Pisum sativum and bottle gourd Lagenaria siceraria: Characterization and antibacterial properties. Front Environ Sci. 2022; 10:941554.
12. Patra JK, Das G, Shin HS. Facile green biosynthesis of silver nanoparticles using Pisum sativum L. outer peel aqueous extract and its antidiabetic, cytotoxicity, antioxidant, and antibacterial activity. Int J Nanomedicine. 2019; 14:6679-90.
13. Hadrich F, Arbi ME, Boukhris M, Sayadi S, Cherif S. Valorization of the peel of pea: Pisum sativum by

evaluation of its antioxidant and antimicrobial activities. J Oleo Sci. 2014; 63(11):1177-83.
14. El-Feky AM, Elbatanony MM, Mounier MM. Anti-cancer potential of the lipoidal and flavonoidal compounds from Pisum sativum and Viciafaba peels. Egypt J Basic Appl Sci. 2018; 5(4):258-64.
15. Naganathan K., Thirunavukkarasu S. Greenway genesis of silver nanoparticles using multiple fruit peels waste and its antimicrobial, anti-oxidant and anti-tumor cell line studies. IOP Conf. Series: *Mater Sci Eng.*2017; 191(1): 012009.
16. Stylianopoulos T. EPR-effect: utilizing size-dependent nanoparticle delivery to solid tumors. Ther Deliv. 2013; 4 (4):421-3.
17. Basavegowda N, Mishra K, Thombal RS, Kaliraj K, Lee YR. Sonochemical green synthesis of yttrium oxide (Y2O3) nanoparticles as a novel heterogeneous catalyst for the construction of biologically interesting 1, 3-thiazolidin-4-ones. Catal Letters. 2017; 147:2630-9.
18. Boo H, Park J, Lee M, Kwon S, Kim H. In vitro cytotoxicity against human cancer cell and 3T3-L1 cell, total polyphenol content and DPPH radical scavenging of codonopsis lanceolata according to the concentration of ethanol solvent. Korean J. Plant Res. 2018; 31: 195-201.
19. Kwon MJ, Oh E, Lee S, Roh MR, Kim SE, Lee Y, et al. Identification of novel reference genes using multiplatform expression data and their validation for quantitative gene expression analysis. PloS one. 2009; 4(7): e6162.
20. Alyami NM, Alyami HM, Almeer R. Using green biosynthesized kaempferol-coated sliver nanoparticles to inhibit cancer cells growth: An in vitro study using hepatocellular carcinoma (HepG2). Cancer Nanotechnology. 2022; 13(1):26.
21. Jegadeeswaran P, Shivaraj R, Venckatesh R. Green synthesis of silver nanoparticles from extract of Padina tetrastromatica leaf. Dig J Nanomater. Biostruct. 2012; 7(3):991-8.
22. Choudhari S, Bhandari S. Green Synthesis of Silver Nanoparticles Using Phyllanthus emblica and Vaccinium oxycoccos Extract: Preparation, Characterization, and Antimicrobial Efficacy. ASDJ. 2024; 34(2):14-22.
23. Sastry M, Mayya KS, Bandyopadhyay K. pH Dependent changes in the optical properties of carboxylic acid derivatized silver colloidal particles. Colloids and Surfaces A: Physicochemical and Engineering Aspects. 1997;127 (1-3):221-8.
24. Coates J. Interpretation of infrared spectra, a practical approach. In: Encyclopedia of Analytical Chemistry, RA. Meyers (Ed.). John Wiley& Sons Ltd, Chichester. 2000; 12:10815-37.
25. Faedmaleki F, Shirazi FH, Salarian AA, Ashtiani HA, Rastegar H. Toxicity effect of silver nanoparticles on mice liver primary cell culture and HepG2 cell line. Iran J Pharm Res. 2014; 13(1):235-42.
26.Cardano M, Tribioli C, Prosperi E. Targeting proliferating cell nuclear antigen (PCNA) as an effective strategy to inhibit tumor cell proliferation. Curr Cancer Drug Targets. 2020; 20(4):240-52.
27. Liu S, Chen S, Zeng J. TGF-β signaling: A complex role in tumorigenesis (Review). Mol Med Rep. 2018; 17(1): 699-704.
28. Javed B, Mashwani ZR. Synergistic effects of physicochemical parameters on bio-fabrication of mint silver nanoparticles: structural evaluation and action against HCT116 colon cancer cells. Int. J Nanomed. 2020; 15: 3621-37.
29. Mfouo-Tynga I, El-Hussein A, Abdel-Harith M, Abrahamse H. Photodynamic ability of silver nanoparticles in inducing cytotoxic effects in breast and lung cancer cell lines. Int J Nanomed. 2014; 9(1):3771-80.
30. Martin ME, Reaves DK, Jeffcoat B, Enders JR, Costantini LM, Yeyeodu ST, et al. Silver nanoparticles alter epithelial basement membrane integrity, cell adhesion molecule expression, and TGF-β1 secretion. Nanomedicine. 2019; 21:102070.
31. Eskandari E, Eaves CJ. Paradoxical roles of caspase-3 in regulating cell survival, proliferation, and tumorigenesis. Journal of Cell Biology. 2022; 221(6): e202201159.
32. Jabeen S, Qureshi R, Munazir M, Maqsood M, Munir M, Shah SS, et al. Application of green synthesized silver nanoparticles in cancer treatment—a critical review. Mater Res Express. 2021; 8(9):092001
33. Nishanth RP, Jyotsna RG, Schlager JJ, Hussain SM, Reddanna P. Inflammatory responses of raw 264.7 macrophages upon exposure to nanoparticles: Role of ROS-NFkB signaling pathway. Nanotoxicology.2011; 5(4):502-16.
34. Verano-Braga T, Miethling-Graff R, Wojdyla K, Rogowska-WrzesinskaA, Brewer JR, Erdmann H, et al. Insights into the cellular response triggered by silver nanoparticles using quantitative proteomics. ACS Nano. 2014; 8(3): 2161-75.
35. Gurunathan S, Jeong JK, Han JW, Zhang XF, Park J, Hand Kim JH. Multidimensional effects of biologically synthesized silver nanoparticles in helicobacter pylori, helicobacter felis, and human lung (l132) and lung carcinoma a549 cells. Nanoscale Res. Lett. 2015; 10: 35.
36. Banerjee PP, Bandyopadhyay A, Harsha SN, Policegoudra RS, Bhattacharya S, Karak N, et al. Mentha arvensis (Linn.)-mediated green silver nanoparticles trigger caspase 9-dependent cell death in MCF7 and MDA-MB-231 cells. Breast Cancer (Dove Med Press). 2017; 9:265-78.

37. Sayed R, Sabry D, Hedeab G, Ali H. In Vitro Characterization and Evaluation of Silver Nanoparticles Cytotoxicity on Human "Liver and Breast" Cancer Cells Versus Normal Melanocytes. Egy J Histol, 2019; 42(3): 755-766.
38. Kumari R, Saini AK, Kumar A, Saini RV. Apoptosis induction in lung and prostate cancer cells through silver nanoparticles synthesized from Pinus roxburghii bioactive fraction. J Biol Inorg Chem. 2020; 25(1):23-37.
39. Artiukh L, Povnitsa O, Zahorodnia S, Pop CV, Rizun N. Effect of Coated Silver Nanoparticles on Cancerous vs. Healthy Cells. J Toxicol. 2022; 2022: 1519104.
40. Hembram KC, Kumar R, Kandha L, Parhi PK, Kundu CN, Bindhani BK. Therapeutic prospective of plant-induced silver nanoparticles: application as antimicrobial and anticancer agent. Artificial Cells, Nanomedicine, and Biotechnology. 2018; 46(3):38–51.
41. Kah G, Chandran R, Abrahamse H. Biogenic Silver Nanoparticles for Targeted Cancer Therapy and Enhancing Photodynamic Therapy. Cells. 2023; 12:2012.